14th IMEKO TC10 Workshop on Technical Diagnostics
New Perspectives in Measurements, Tools and Techniques
for systems reliability, maintainability and safety
Milan, Italy, June 27-28, 2016

On the effects of motion blur in vision based 3D vibration monitoring

Alberto Lavatelli [1], Emanuele Zappa [2]

[1] Dept. of Mechanics, Politecnico di Milano, Via La Masa 1 20156 Milano, alberto.lavatelli@polimi.it
[2] Dept. of Mechanics, Politecnico di Milano, Via La Masa 1 20156 Milano, emanuele.zappa@polimi.it

Abstract **- This paper addresses the problem of motion blur when 3D vibration monitoring is performed by means of vision based measurement methods. Starting from an original analytic model developed previously by the authors, the paper discusses the effects of acquisition parameters on the final measurement accuracy. Consequently the paper proposes an experimental method in order to asses the presented theoretical framework as well as the accuracy of a generic vision based vibration monitoring system.**

Keywords: vision based vibration monitoring; uncertainty analysis; motion blur;

1. INTRODUCTION

Vibration measurement plays an essential role in structural health monitoring, manufacturing process and automation systems. During the last two decades, it has been possible to develop several non-contact methodologies able to measure vibration remotely, thanks to the continuous improvement of the hardware, in terms of calculation power and size. This dissertation will focus onto the application of imaging techniques to 3D vibration monitoring.

The task of monitoring vibrations by means of image processing techniques may be carried out through several techniques. Regardless the specific methodology, everything starts from recording a moving target with one ore more cameras. The mechanism of image formation implies that the scene including a vibrating measurand is recorded for a finite amount of time, indicated as exposure time. The superimposition of measurand relative motion in terms of instantaneous velocity and acceleration during the exposure time always generates motion blur. Hence the effect of motion blur can be significant or negligible, but is always embedded in the image of a vibrating target. As a consequence motion blur is a contribute to uncertainty that should be evaluated with a proper model.

2. STATE OF THE ART

The use of imaging devices as displacement transducers was firstly proposed in almost-static applications, where the effect of target motion during the exposure time can be neglected. Thanks to technology improvements, the applications of vision-based measurement to dynamic applications have been increasing in the last years. The available image resolutions and the high grabbing frequencies allow to acquire high-speed moving object and to perform dynamic analysis of vibrating objects. When imaging devices are used in dynamic applications the quantification of the measurement uncertainty becomes more complex with respect to the static case [1]. Therefore, in actual vision based vibration monitoring applications the available uncertainty estimation techniques are not always able to provide reliable results as shown in [2][3]. A good displacement estimation will indeed depend on the dynamic camera parameters, such as grabbing frequency, but, most of all, the exposure time that must be settled to a proper value in order to limit the phenomenon of motion blur. For these reasons, many experimenters found a good solution in boosting lighting and selecting very low exposure times in order to shoot the vibrating object in approximately static conditions [4]. Unfortunately it is not possible to work in those conditions for every measurement task. For instance, in the relevant field of structure monitoring, the application of vision measurement system often requires to work with natural light [5]. Consequently the exposure time can not be set arbitrarily, hence it plays a relevant role and the source of uncertainties peculiar of dynamic measurements starts to be relevant [6]. In conclusion, a wide history of applications indicates clearly that modelling the uncertainty in dynamic conditions implies the understanding of the role played by the interaction between exposure time and the velocity of the vibrating object [7].

3. LINEAR CONVOLUTION MODEL

In order to address the problem of quantifying the effects of motion blur in vibration analysis, it is possible to model motion blur with the linear convolution theory [8] [9]. In fact the blurred image is equal to the original one convolved with a square pulse signal. Then the authors evaluated uncertainty when monitoring a vibrating target as the normalized discrepancy between the actual position of the center of gravity of a circular marker $x_r(t_0) = A_0 sin(\omega_0 t_0)$ and the vision measured one $x_M(t_0)$.

$$\varepsilon = \frac{x_M(t_0) - x_r(t_0)}{x_r(t_0)} \tag{1}$$

Using the convolution theory, $x_M(t_0)$ is the result of the convolution integral between the motion of the measurand and the acquisition window $w(t)$ (consisting in a rectangular pulse starting at t_0 with length equal to the exposure time t_{sh}). Since motion is a sine wave, it is possible to expand the

convolution integral and retrieve the expression of equation (2).

$$x_M(t_0) - x_r(t_0) = \frac{1}{2} A_0 \omega_0 \cdot cos(\omega_0 t_0) \cdot t_{sh} + \Delta x \quad (2)$$

Consequently the expression of equation (1) has been expanded, resulting in the formula of equation (3) [10]. The analysis takes into account the contributions of uncertainty due to static factors and the ones due to dynamic factors.

$$\varepsilon(A_0) = \frac{\Delta x}{2 \cdot A_0} + \frac{A_0 \cdot \Delta x^{-1} \cdot \cos(\phi_0) \cdot 2\pi \cdot E2PR}{2A_0 \cdot \Delta x^{-1} \cdot \sin(\phi_0) + L_0} \quad (3)$$

Equation (3) is composed by two terms: the first one deals with the static performances of the system, hence it is indicated as ε_S, the second one deals with motion blur phenomenon, hence it is a dynamic contribute indicated as ε_D. The whole expression of uncertainty depends on the following parameters:

- Vibration amplitude A_0 (in mm)
- Spatial resolution Δx (in mm/px)
- Phase of motion at shutter opening $\phi_0 = \omega_0 t_0$
- Size of marker L_0 (in pixels)
- The ratio between exposure time and vibration period $E2PR = \frac{1}{2\pi} \omega_0 \cdot t_{sh}$

The here listed parameters are all available or at least estimable by the experimenter, hence this model is suited to be applied in real contexts. For what concerns the derivation of the previous model, the authors refer to the publication [10].

4. MODEL ANALYSIS

The model of equation (3) can be seen as a parametric function that describes the behavior of normalized discrepancy (see eq.1) as a function of vibration amplitude in the form $\varepsilon(A_0)$. Having fixed all parameters (Δx, ϕ_0, L_0, $E2PR$), it is possible to draw the curve of uncertainty in Fig. 1, where the curve of ε is plotted together with ε_S and ε_D. The analysis of the curves of Fig. 1, highlights that as vibration amplitude grows, the weight of uncertainty due to resolution diminishes while the motion blur contribute grows monotonically. As a consequence the combination of the two results in a bowel shaped curve. Then it is possible to analyze how the model reacts to changes in the acquisition and measurand parameters.

A. Changing spatial resolution

Altering the spatial resolution Δx will affect the static behavior of the system. The contribute $\varepsilon_S(A_0)$ draws a line in the log-log plane, with constant slope in Fig. 2. As Δx grows, the line rigidly translates up and reaches higher level of uncertainty.

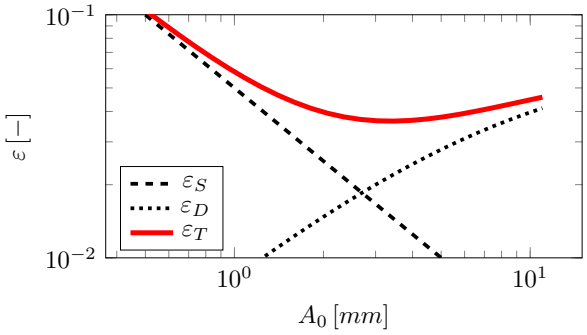

Fig. 1. Behaviour of ε as vibration amplitude changes.

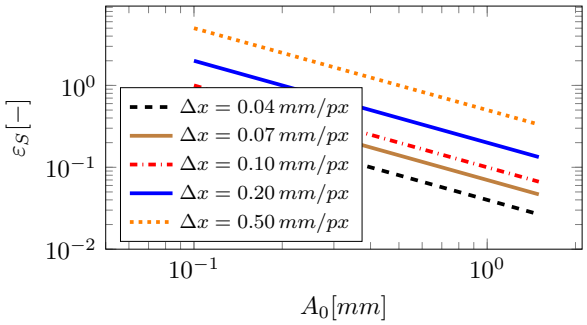

Fig. 2. Behaviour of $\varepsilon_S(A_0)$ as resolution changes.

B. Changing phase of motion

The instantaneous velocity of measurand changes with the phase of motion ϕ_0 at the beginning of exposure. For a fixed value of exposure time , the higher is the marker velocity, the bigger are the effects of motion blur. In Fig. 3 the curve $\varepsilon_D(A_0)$ is plotted at different value of phase of motion.

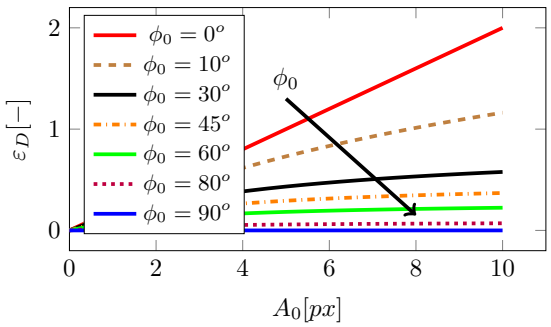

Fig. 3. Behavior of $\varepsilon_D(A_0)$ as ϕ_0 changes.

More precisely, as phase grows from 0 to 90, instantaneous speed decreases, hence the sensitivity to motion blur is lower. This situation suggests that sampling motion at peaks is a good practice since the dynamic component of discrepancy would be canceled since the

length of convolution window $w(t)$ is identically equal to zero. This statement is true only while $E2PR$ is small enough to approximate the reference motion with its Taylor polynomial. However frame grabbing at peaks remains a good choice since, among all the points of a sinusoidal reference motion, it is the one which minimizes motion blur, even at high exposure ratio. Reporting the behavior of $\varepsilon(A_0)$ when ϕ_0 changes in Fig. 3, it is possible to see the existence of two limit curves:

- when $\phi_0 = 0°$, $\varepsilon(A_0)$ is equal to $\frac{2\pi \cdot E2PR}{\Delta x L_0} \cdot A_0$
- when $\phi_0 = 90°$, $\varepsilon(A_0)$ is identically equal to zero

In particular when speed is maximum the curve $\varepsilon(A_0)$ degenerates on a line. This theoretical evidence is also experimentally documented in literature [5].

C. Changing marker size

Changing the size of marker L_0 plays a relevant role in setting the sensitivity of the system to motion blur uncertainty ε_D . It is possible to identify two limit configurations in equation (4): the bigger is the marker, the higher are the chances to fall in a situation where the effects of motion blur are linear.

$$\varepsilon_D \approx \begin{cases} A_0 \cdot \frac{2\pi cos(\phi_0) \cdot E2PR}{L_0 \Delta x} & \forall L_0 \gg \frac{A_0}{\Delta x} \\ \frac{\pi \cdot E2PR}{tan(\phi_0)} & \forall L_0 \ll \frac{A_0}{\Delta x} \end{cases} \quad (4)$$

Having fixed all other parameters, it is possible to plot the curves of $\varepsilon_D(A_0)$ when marker size L_0 changes in Fig. 4. It is possible to see that the bigger is the size of the marker, the lower is the value of uncertainty as well as the linearity of the system. Marker size in fact, reduces the sensitivity to losses of edge strength and prevents loss of contrast due to smearing. As L_0 decreases, the curve tends asymptotically to the value of $\frac{\pi \cdot E2PR}{tan(\phi_0)}$.

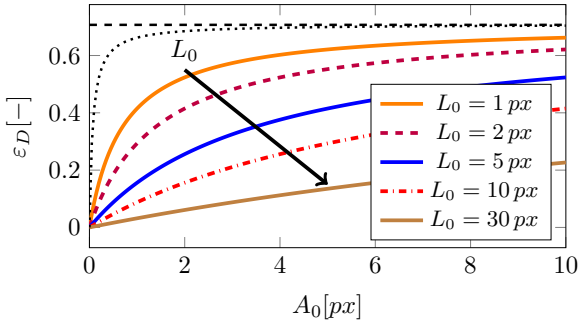

Fig. 4. Behavior of $\varepsilon_D(A_0)$ as L_0 changes.

D. Changing exposure to period ratio E2PR

The influence of parameter is quite relevant: an increment in $E2PR$ is always negative for the accuracy of the system. In fact, from a physical point of view, $E2PR$ is a measure of how much a moving target is to be considered as a still one during the exposure time: the lower the value, the lower is the risk to have motion blur. From a mathematical point of view, in equation (3) the parameter $E2PR$ is a mere amplification factor of ε_D, so, in the end it steers the curve up or down, proportionally to its value (fig. 5). This demonstrates that it is always good to boost the illumination of the scene in order to keep exposure time as low as possible [11].

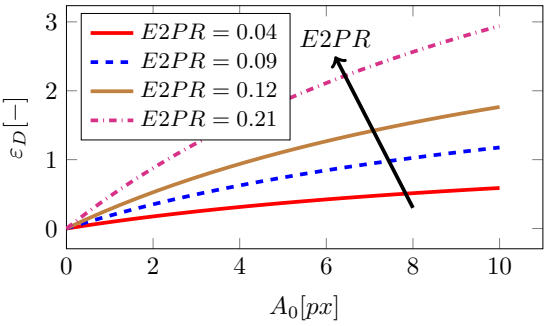

Fig. 5. Behavior of $\varepsilon_D(A_0)$ as $E2PR$ changes.

5. EXPERIMENTAL VALIDATION

The model formulated above has been derived theoretically. In order to verify its physical coherence, a dedicated experimental test was designed. The test stand had to provide a multi dimensional dynamic vibrational motion (in the 15-25 Hz band) with varying amplitude and a reference measurement which is supposed to be more accurate than the general vision system. In this section the design of test-stand, the measurement chain and the signal processing will be discussed. In the end, final data that validate the model will be presented.

A. Providing complex 3D vibration patterns

In order to create a testing system able to produce the desired mechanical vibrations, the choice was made for a flexible mechanical structure. This choice is claimed to minimize the cost of motion actuation and boost the repeatability performances. The drawback is that vibration amplitude is not directly controllable and it may be hard to achieve a complex motion. In order to cope with these limits, a cantilever beam with the peculiarity of having slightly different moments of inertia along the two principal section axis was designed. To achieve varying amplitude, the natural structural damping is used. As a consequence the experimental procedure is based on decay tests. In order to obtain a beam with slightly different moments of inertia for the two axis of symmetry, the solution was found in a square tube commercial profile (Fig. 6) with height h =40 mm and thickness t =3 mm made out of steel (length 1400 mm).

Then inertia and frequency tuning has been reached by CNC surface milling. In fact removing a defined amount

of material from the faces of a square beam produces a reduction in moment of inertia relative to the axis at which surfaces are normal to (Fig. 6).

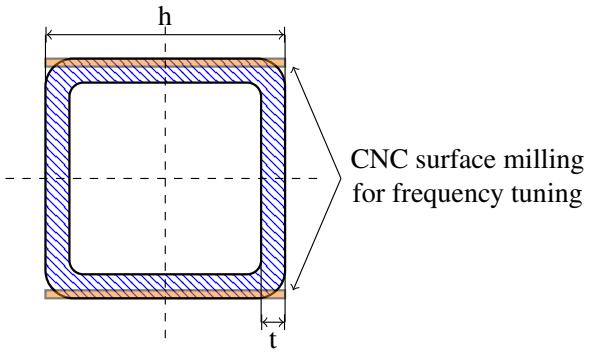

Fig. 6. Frequency tuning procedure.

The selection of milling depth necessary to achieve complex motion has been computed with a FEM model. The beam was modeled with shell elements, then the shell thickness has been changed until the trajectory of beam tip under impulsive excitation was rather complex, with the tip drawing orbit-like trajectories (Fig. 7). This was achieved with a milling depth Δt equal to $0.56\,\mathrm{mm}$. The predicted natural frequencies for the first two flexural modes are $21.6\,\mathrm{Hz}$ and $22.9\,\mathrm{Hz}$.

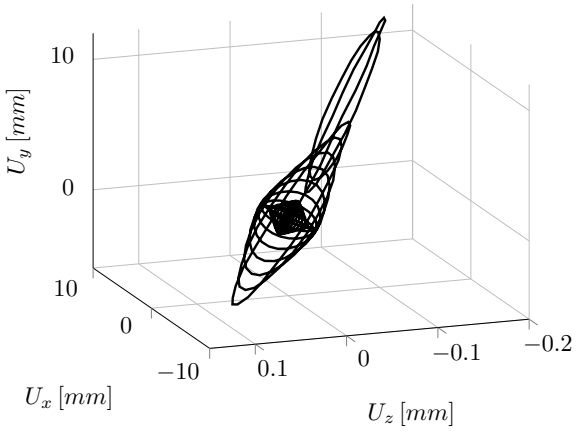

Fig. 7. FEM simulated beam tip trajectories: impulsive force response.

In order to achieve variable vibration amplitude, the natural structural damping of the cantilever beam has been exploited. Natural damping is low enough to ensure a smooth and slow decay, hence, it is possible to test the beam in quasi-stationary linear conditions. The motion is excited with a position forcing: the beam tip is moved and constrained a few millimeters away from its equilibrium position, then the beam tip is released. In this way the beam tip vibrates freely without exciting high frequency modes.

B. Measurement system

The motion of beam tip is measured by a stereovision rig consisting of two AVT Marlin F131B (focal length of $8\,\mathrm{mm}$) cameras mounted on a aluminum frame together with dimmerable LED lighting (Smart Vision Lights ODS75) and two triangulation lasers ($\mu\varepsilon$ OptoNCDT 1302-50) aligned with the cantilever beam, as shown in Fig. 8. In this vibrations are monitored by two measurement systems: the uncertainty of the vision system is judged over the reference measurement offered by triangulation lasers, which are affected by negligible uncertainty respect to the stereo vision rig used [12].

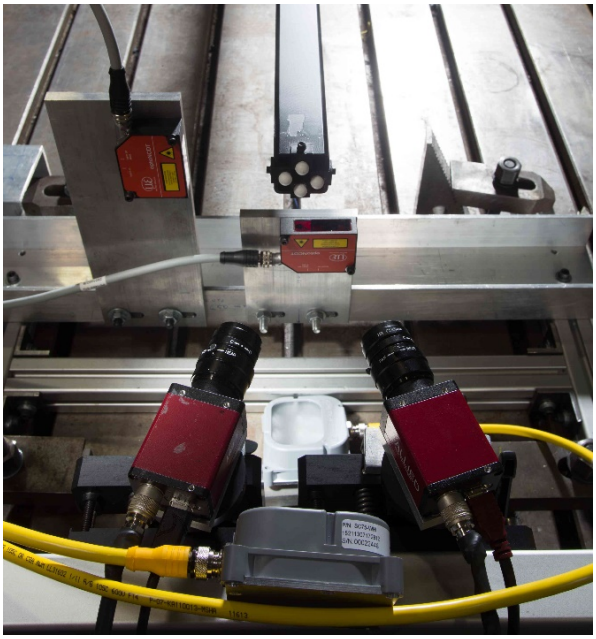

Fig. 8. Final test stand layout.

A critical issue to be solved in this layout is the synchronization problem among all the above listed instruments. In fact it is necessary to:

- ensure that the images coming from the left and right camera are acquired at the same time (synchronous shutter),
- ensure that the laser signal is acquired in synchronous with cameras, or, at least, with a common time base.

This result is achieved by using the timing scheme displayed in Fig. 9, where a common time base drives both the camera acquisition (shutter begins with rising edge) and the ADC conversion of the laser signal (acquisition begins with rising edge). The two cameras share the same trigger signal. Meanwhile, the analog acquisition is paced at a frequency which is an integer multiple of the camera sampling frequency.

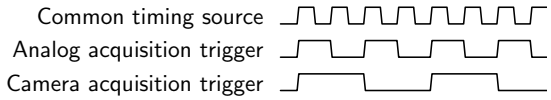

Fig. 9. Timing table of signal acquisition procedure

C. Image processing technique

After stereo vision rig calibration, it is possible to measure the motion of beam tip using the well known Stereo Vision Blob Analysis methodology (SVBA). In brief, SVBA is based on a procedure highlighted by Hartley and Zisserman in [13], where 3D position of an object is retrieved using the tracked position of a marker in each single frame (left and right) to reconstruct epipolar geometry. Since the problem is overdetermined (3 spatial variables to be retrieved after 4 known coordinates in the pixel space) singular value decomposition (SVD) factorization is necessary to calculate the 3D position of a single marker.

As shown in Fig. 8, the beam tip is equipped with a marker consisting in 4 white spheres distributed around the center of gravity of the beam section. This produces 4 bright blobs in the acquired image. The segmentation of blobs inside the acquired images is done by a fixed threshold binarization. Each binary image is then labeled and the center of gravity of each blob is computed. Eventually it was possible to recover the position of beam tip by averaging the position of the 4 blobs centroids.

D. Signal analysis

The measurement system specified above measures the motion of the beam tip in vertical direction y and horizontal direction x. A first set of raw signals (Fig 10) is composed by the one retrieved by the vision system $x_{vis}(t)$, $y_{vis}(t)$, the second set includes the laser data $x_{las}(t)$, $y_{las}(t)$. The two signals are acquired at different sampling frequencies, $1\,\mathrm{kHz}$ for the lasers, while the highest camera frame rate is $100\,\mathrm{Hz}$. But, given the common time base shown in Fig. 9, it is possible to adequately re-sample them in order to have for each measurement coming from the vision system a coherent measurement from the triangulation lasers. Furthermore, the laser raw signal comes with electric noise, as a consequence the acquired data have been processed with a low pass filter.

At this point, it is possible to calculate vibration amplitude envelopes for lasers and vision system from re-sampled signals with the help of RMS windowing (length $1100\,\mathrm{ms}$ in order to accomodate about 25 periods, $500\,\mathrm{ms}$ overlap). The result of this processing step is shown in Fig.11, where it is possible to see both the decaying behavior of free vibrations and the differences among the two measurement systems. Then the difference between the amplitude envelopes of lasers and vision system, gives the measurement discrepancy. Then the ratio between discrepancy and laser amplitude returns several data points of the normalized discrepancy $\varepsilon(A_0)$ (eq.(3)) as a function of vibration amplitude (Fig. 12).

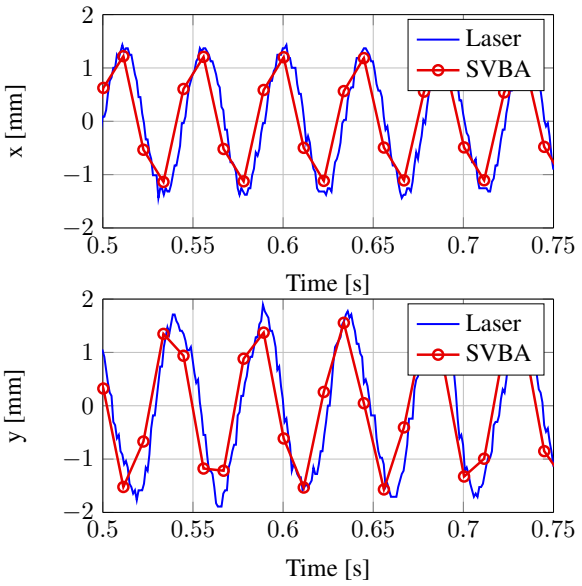

Fig. 10. Raw signals coming from the test stand for exposure time of $4.4\,\mathrm{ms}$ at 90 fps

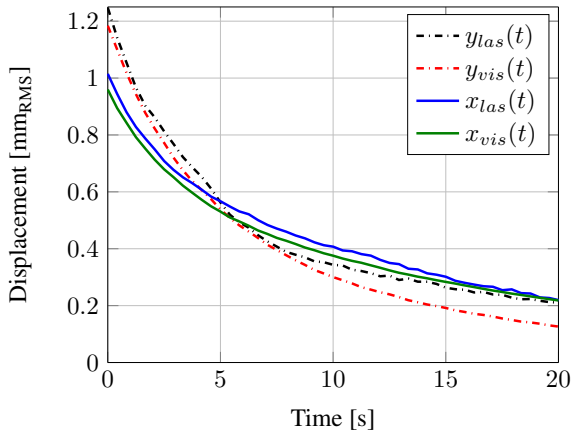

Fig. 11. Vibration RMS amplitude comparison between laser and stereo vision, for exposure time of $4.4\,\mathrm{ms}$ at 90 fps

E. Validation tests

Data retrieved during the tests, represent a cloud of $\varepsilon(A_0)$ values. Consequently, it is possible to fit this point cloud with the model of equation (3). The fitting procedure is quite elaborated since the fit function is non-linear. For this task the *Matlab* function `lsqcurvefit` implements the non linear least square sense fitting methodology using trust-region-reflective algorithm as described in [14]. For this algorithm, the fitting function is formulated as in equation (5).

$$\varepsilon_i(A) = \frac{k_{1,i}}{A} + \frac{k_{2,i} \cdot A}{k_{3,i} \cdot A + k_{4,i}} \tag{5}$$

The fit procedure returns the set of fit parameters $\langle k_{1,i}\,;\,k_{2,i}\,;\,k_{3,i}\,;\,k_{4,i}\rangle$ which are a combination of the physical parameters of equation (3). The i index indicates that the resulting fit parameters are related to the i-th set of data.

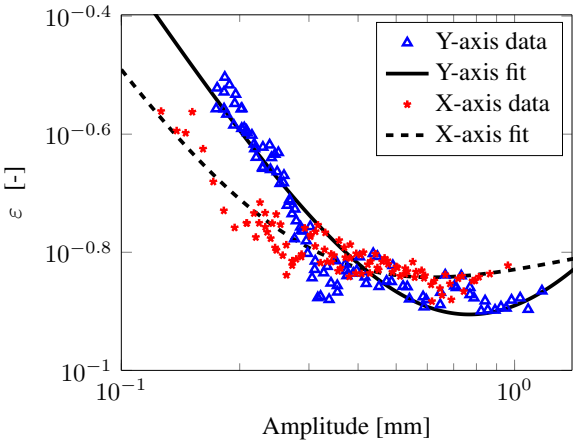

Fig. 12. Experimental data and model when $E2PR \approx 0.092$.

In Fig. 12 it is possible to see that qualitatively the model fits the data. From a quantitative point of view, goodness of fit can be judged through the coefficient of determination R^2 and the analysis of residuals [15]. In several working conditions (with different experimental parameters), the model were able to fit the data with $R^2 \geq 0.87$. The residuals have been successfully tested for normality with the Anderson-Darling method. As a consequence it is possible to state that the proposed model is able to describe correctly the uncertainty behavior of an actual vision based measurement system.

6. CONCLUSION

In a previous publication, the authors presented a novel theoretical model to describe uncertainty in the context of vision based 3D vibration monitoring [10]. In this work, the sensitivity of the proposed theory to the main experimental parameters is discussed. In addition, the experimental validation is presented in details, in order to propose a benchmark procedure for the characterization of vision based vibration monitoring systems.

REFERENCES

[1] G. Busca, G. Ghislanzoni, and E. Zappa, "Indexes for performance evaluation of cameras applied to dynamic measurements," *Measurement: Journal of the International Measurement Confederation*, vol. 51, no. 1, pp. 182–196, 2014.

[2] P. Poozesh, J. Baqersad, C. Niezrecki, E. Harvey, and R. Yarala, "Full-field inspection of a utility scale wind turbine blade using digital image correlation," in *CAMX 2014 - Composites and Advanced Materials Expo: Combined Strength. Unsurpassed Innovation*, The Composites and Advanced Materials Expo (CAMX), 2014.

[3] P. Poozesh, J. Baqersad, C. Niezrecki, and P. Avitabile, *Advancement of Optical Methods in Experimental Mechanics, Volume 3: Proceedings of the 2015 Annual Conference on Experimental and Applied Mechanics*, ch. A Multi-camera Stereo DIC System for Extracting Operating Mode Shapes of Large Scale Structures, pp. 225–238. Cham: Springer International Publishing, 2016.

[4] T. Siebert, T. Becker, K. Spiltthof, I. Neumann, and R. Krupka, "High-speed digital image correlation: error estimations and applications," *Optical Engineering*, vol. 46, no. 5, pp. 051004–051004–7, 2007.

[5] P. Olaszek, "Investigation of the dynamic characteristic of bridge structures using a computer vision method," *Measurement: Journal of the International Measurement Confederation*, vol. 25, no. 3, pp. 227–236, 1999.

[6] G. Busca, A. Cigada, P. Mazzoleni, M. Tarabini, and E. Zappa, "Static and dynamic monitoring of bridges by means of vision-based measuring system," in *Conference Proceedings of the Society for Experimental Mechanics Series*, vol. 3, pp. 83–92, 2013.

[7] C. Niezrecki, P. Avitabile, C. Warren, P. Pingle, and M. Helfrick, "A review of digital image correlation applied to structura dynamics," *AIP Conference Proceedings*, vol. 1253, no. 1, pp. 219–232, 2010.

[8] E. Zappa, P. Mazzoleni, and A. Matinmanesh, "Uncertainty assessment of digital image correlation method in dynamic applications," *Optics and Lasers in Engineering*, vol. 56, pp. 140–151, 2014.

[9] E. Zappa, A. Matinmanesh, and P. Mazzoleni, "Evaluation and improvement of digital image correlation uncertainty in dynamic conditions," *Optics and Lasers in Engineering*, vol. 59, pp. 82–92, 2014.

[10] A. Lavatelli and E. Zappa, "Modeling uncertainty for a vision system applied to vibration measurements," *IEEE Transactions on Instrumentation and Measurement*, vol. PP, no. 99, pp. 1–9, 2016. DOI:10.1109/TIM.2016.2541359.

[11] T. Schmidt, J. Tyson, and K. Galanulis, "Full-field dynamic displacement and strain measurement using advanced 3d image correlation photogrammetry: Part 1," *Experimental Techniques*, vol. 27, no. 3, pp. 47–50, 2003.

[12] A. Donges and R. Noll, *Laser Measurement Technology: Fundamentals and Applications*, ch. Laser Triangulation, pp. 247–278. Berlin, Heidelberg: Springer Berlin Heidelberg, 2015.

[13] R. I. Hartley and A. Zisserman, *Multiple View Geometry in Computer Vision*. Cambridge University Press, ISBN: 0521540518, second ed., 2004.

[14] J. Dennis and R. Schnabel, *Numerical Methods for Unconstrained Optimization and Nonlinear Equations*. Society for Industrial and Applied Mathematics, 1996.

[15] S. Glantz and B. Slinker, *Primer of Applied Regression and Analysis of Variance*. McGraw-Hill, Health Professions Division, 1990.